AIAA SciTech Forum
23-27 January 2023, National Harbor, MD & Online
AIAA SCITECH 2023 Forum

10.2514/6.2023-1442

Quadrotor Flight Envelope Protection while Following High-Speed Trajectories: a Reference Governor Approach

Rick Schieni*[1], Chengwei Zhao †[1], John Barreira‡[1], Michael Malisoff§[2], and Laurent Burlion¶[1]
[1]*Rutgers, The State University of New Jersey, New Brunswick, NJ, 08901, USA*
[2]*Louisiana State University, Baton Rouge, LA 70803-4918, USA*

Aerodynamic effects can become dangerous when a drone follows a path at high speed even in the absence of wind. This paper studies a method to ensure that a quadrotor drone follows a 2D high-speed trajectory in the presence of safety constraints. A reference governor control is implemented to make the drone follow its trajectory, while respecting a set of constraints that includes polynomial constraints when aerodynamic effects are modelled. The method is based on a recent state space augmentation technique that converts polynomial constraints into linear constraints. For the first time, this state augmentation technique is applied to flight envelope protection for tracking high-speed trajectories using a reference governor to alter the reference trajectory to protect the flight envelope. Simulation results for the proposed algorithms are reported when a drone follows a circular trajectory with increasing speed.

Nomenclature

e_1, e_2, e_3	=	inertial frame
x, y, z	=	3D position of the drone with respect to the inertial frame, m
v_x, v_y, v_z	=	linear velocities expressed in the inertial frame, m/s
m	=	drone mass, kg
g	=	gravitational acceleration, m/s^2
c	=	mass normalized collective thrust, m/s^2
θ, ϕ, ψ	=	Euler angles (pitch,roll,yaw), rad
p, q, r	=	angular velocities expressed in the body frame, rad/s
J_{xx}, J_{yy}, J_{zz}	=	inertia coefficients of the diagonal inertia matrix J, $kg.m^2$
τ_1, τ_2, τ_3	=	torque produced by the propellers in the body frame, Nm
M_{eff}	=	control effectiveness matrix
T_i	=	individual thrust produced by the i-th propeller, $i \in \{1, 4\}$, N
X_{lon}	=	column vector $[v_x; \theta; q]$, [m/s; rad; rad/s]
X_{lat}	=	column vector $[v_y; \phi; p]$, [m/s; rad; rad/s]

I. Introduction

Quadrotor unmanned aerial vehicles (or UAVs) are some of the most popular UAV platforms as their underactuated and unstable dynamics allow them to perform aggressive flight maneuvers. Controlling quadrotor drones has traditionally been done by neglecting aerodynamic effects which only become relevant outside of hover conditions [1]. Consideration of aerodynamic effects has recently become a popular research area, as these can no longer be overlooked when a drone is operating at high speed and/or in high wind conditions. During high speed flight, quadrotor drones are subjected to aerodynamic effects such as rotor drag, blade flapping, and thrust variation due to induced velocity changes [2].

Most of the previous research on the aerodynamics of quadrotor UAVs has been based on helicopter aerodynamics [3, 4]. In [5], first order aerodynamic effects were investigated, while in [6] the effects of drag and thrust power were

*Graduate Research Assistant, MAE Department, rick.schieni(at)rutgers.edu
†Graduate Research Assistant, MAE Department, chengwei.zhao(at)rutgers.edu
‡Graduate Research Assistant, MAE Department, jdb307(at)scarletmail.rutgers.edu
§Full Professor, Department of Mathematics, malisoff(at)lsu.edu
¶Assistant Professor, MAE Department, laurent.burlion(at)rutgers.edu, AIAA Senior Member.

investigated near hover conditions. A drag-augmented control scheme for quadrotor drones was developed in [7]. Techniques which take drag into account near hover conditions are presented in [8–10]. Blade flapping during the ascent and descent stages of flight are considered in the control design in [11]. Increasing flight speeds and the resulting aerodynamic effects from blade flapping and thrust variation were addressed in [12]. In [13], an analysis of blade flapping and thrust variation is taken into consideration when developing models and control methods for quadrotor UAVs. Rotor drag effects in quadrotor drones were studied in [7, 9, 14] and the same effects were studied in vehicles capable of vertical take-off and landing (or VTOLs) in [15]. The authors in [1] developed a control method for improving trajectory tracking while considering rotor drag, an improvement over previous methods which treated aerodynamic effects as disturbances which led to increasing trajectory following error as speed increased. By contrast, this work will consider the aerodynamics in the control of a quadrotor while ensuring that the safe flight envelope (or SFE) is protected.

The capabilities of an aircraft in terms of speed, load, and altitude are referred to as its flight envelope. Ensuring that an aircraft remains within its flight envelope is essential to prevent loss of control (or LoC). Since quadrotor drones are unstable, preventing LoC is crucial to ensure their safety [16]. A SFE must be predicted accurately for an aircraft to prevent LoC. Envelope protection currently entails preventing specific constraint violations [17]. Existing literature on defining SFEs for commercial fixed-wing aircraft is available [18–20] but there is little research on the SFE for quadrotor drones. In [21], the authors predict the SFE for a quadrotor moving at high speeds using Monte Carlo simulations.

By contrast, the present work is devoted to methods that are based on reference governors. Reference governors are add-on schemes which modify the reference signal that is fed into the nominal controller to satisfy constraints [22]. Should the constraints be satisfied by the original reference signal, the reference governor is inactive. Since LoC is to be avoided and additional safety constraints must be satisfied during quadrotor flight, a reference governor approach is employed in this work to ensure constraint satisfaction. Conventional reference governors are based on the maximum output admissible set (or MOAS) which is the set of all initial states and constant reference commands for which the ensuing response satisfies the constraints. The computation of the MOAS gives a forward invariant set which provides a safe set that must contain the state at all times. Reference governor approaches have been used in different applications such as automotive applications [23] (including rollover avoidance [24, 25]), as well as constrained control of UAVs [26]. With the MOAS providing a safe set in which the state of the system may exist, invariant inner approximations of this set, represented by a finite number of inequalities, can be computed easily when both the system dynamics and output constraints are linear. A design for a reference governor for linear systems with polynomial constraints and constant reference commands was developed in [27]. This approach augmented the system state to include the output signal from the reference governor and the constant reference command. The Kronecker product was then used to embed the linear system into another higher dimensional linear system which encompassed the state of the original linear system plus its higher order powers. Originally polynomial constraints would become linear in terms of the new extended state. The approach was shown to successfully satisfy linear state constraints and polynomial actuator constraints in [28].

In this paper, this state augmenting reference governor approach is employed to control a quadrotor drone at high speeds and therefore, subject to aerodynamic effects. This new application was beyond the scope of previous research on this control problem. The reference governor ensures constraint satisfaction, to protect the SFE. The drone model including aerodynamic effects is first presented followed by an explanation of the tracking control method. Propeller thrust limitations are then reformulated as polynomial quadratic constraints which must be satisfied. The modifications to the traditional reference governor scheme to handle polynomial constraints are then reviewed. Lastly, simulations in which a quadrotor drone follows a circular trajectory at increasing speeds are presented. It is shown that the control methodology developed in this paper is capable of controlling a drone as it follows a circular trajectory at increasing speeds in the presence of aerodynamic effects and that the drone can safely stop when it becomes dangerous to track it.

II. Problem formulation

A. Modeling

As was proposed in [7], this paper considers the quadrotor model of [1] assuming no wind, rigid propellers, and no dependence of the rotor drag on thrust. Thrust is modelled as in [2]. As the vehicle moves in a direction, the advancing blade produces a larger relative air velocity than the retreating blade. This causes aerodynamic forces depending on air-velocity to be greater on the advancing blade than the retreating blade. The force imbalance leads to nonzero net forces and torques on the vehicle [7, 9, 29]. The translation equations of motion involving aerodynamic effects are

$$\dot{v} = -ge_3 + cRe_3 - RDR^T v - RC\Omega$$

where $v = [v_x\ v_y\ v_z]^T$ is the velocity, R is the rotation matrix representing the quadrotor's orientation, and $\Omega = [p\ q\ r]^T$ is the angular velocity. The rotational equations of motion are given by

$$J\dot{\Omega} = -\Omega \times J\Omega - \tau_G + \tau - AR^T v - B\Omega$$

where τ_G indicates gyroscopic torques from the propellers and $\tau = [\tau_1\ \tau_2\ \tau_3]$. The matrix D incorporates the effects of the force imbalance as a result of the difference of air-velocities between the advancing and retreating blades. The constant matrices A and B encapsulate the effects of rotor drag and blade flapping on the rotation of the vehicle. This work considers the aforementioned model but simplifies it by assuming:

- the propellers are rigid (i.e., $C = 0$),
- the collective thrust remains equal to the commanded collective thrust,
- the yaw angle ψ and its derivatives remain equal to 0,
- the drone flies at a constant altitude z,
- the pitch and roll angles are small all the time, and
- the inertia matrix is diagonal and $J_{xx} = J_{yy}$.

Under these approximations, the rotation matrix is approximated by the matrix R that is defined by

$$R = \begin{bmatrix} 1 & 0 & \theta \\ 0 & 1 & -\phi \\ -\theta & \phi & 1 \end{bmatrix} \tag{1}$$

and the following equations of motion for the quadrotor were derived by keeping only the linear and quadratic terms:

$$\dot{x} = v_x \tag{2}$$

$$\dot{y} = v_y \tag{3}$$

$$\dot{v}_x = g\theta - d_x v_x \tag{4}$$

$$\dot{v}_y = -g\phi - d_y v_y \tag{5}$$

$$\dot{\phi} = p \tag{6}$$

$$\dot{\theta} = q \tag{7}$$

$$J_{xx}\dot{p} = \tau_1 - a_{11}v_x - a_{12}v_y - a_{13}(\theta v_x - \phi v_y) - b_{11}p - b_{12}q \tag{8}$$

$$J_{yy}\dot{q} = \tau_2 - a_{21}v_x - a_{22}v_y - b_{21}p - a_{23}(\theta v_x - \phi v_y) - b_{22}q \tag{9}$$

The aerodynamic effects are captured in the terms which depend on d_x and d_y and matrices $A \in \mathbb{R}^{3\times3}$ and $B \in \mathbb{R}^{3\times3}$. Here, $A = [a_{ij}]$, and d_x and d_y are the components of D which are mass-normalized rotor-drag coefficients reflecting the force imbalance on the vehicle. Considering the assumptions regarding constant altitude z and from the assumptions regarding yaw that $\psi = r = 0$ all the time, the following equalities hold:

$$\begin{aligned} \dot{v}_z = 0 &= -g + c + d_x\theta v_x - d_y\phi v_y \\ \ddot{\psi} = 0 &= \tau_3 - a_{31}v_x - a_{32}v_y - a_{33}(\theta v_x - \phi v_y) \end{aligned} \tag{10}$$

Eq. (10) gives the mass-normalized collective thrust c and the torque τ_3 applied around the z-axis in the body frame.

B. Trajectory tracking

First a simple change of coordinates is used to decouple the x and y dynamics. The new coordinates

$$\begin{aligned} u_1 &= \tau_1 - a_{11}v_x - b_{12}q - a_{13}(\theta v_x - \phi v_y) \\ u_2 &= \tau_2 - a_{22}v_y - b_{21}p - a_{23}(\theta v_x - \phi v_y) \end{aligned} \tag{11}$$

and applying the change of variables to the equations of motion result in two decoupled systems:

$$\begin{cases} \dot{x} &= v_x \\ \dot{v}_x &= g\theta - d_x v_x \\ \dot{\theta} &= q \\ J_{yy}\dot{q} &= u_2 - a_{21}v_x - b_{22}q \end{cases} \tag{12}$$

and

$$\begin{cases} \dot{y} &= v_y \\ \dot{v}_y &= -g\phi - d_y v_y \\ \dot{\phi} &= p \\ J_{xx}\dot{p} &= u_1 - a_{12}v_y - b_{11}p \end{cases} \tag{13}$$

In the sequel, the decoupled systems in Eq. (12) and Eq. (13) are called the longitudinal and lateral motions, respectively.

1. Longitudinal tracking

For reasons that will become clear later when a reference governor is applied, the trajectory tracking problem in the longitudinal plane is reformulated as a velocity tracking problem where the velocity v_x can track a given time-varying reference. Our analysis will use the output of the following position control loop:

$$v_x^d = -k_p(x - x_c) + \dot{x}_c \tag{14}$$

where $x_c(t)$ is the desired reference trajectory for $x(t)$ to track, and $k_p > 0$ is a tuning gain.

The torque controller is then computed. Using Eq. (12), one obtains the third derivative

$$v_x^{(3)} = \frac{g}{J_{yy}}(u_2 - a_{21}v_x - b_{22}q) - d_x(gq - d_x(g\theta - d_x v_x)). \tag{15}$$

We next specify u_2 such that the v_x dynamics enjoy suitable asymptotic tracking properties, through the specification of roots of a polynomial differential operator. This will entail tracking a reference signal v_{lon}. We pick τ_2 such that the coordinate u_2 in Eq. (11) is

$$u_2 = a_{21}v_x + b_{22}q + \frac{J_{yy}}{g}\left[d_x(gq - d_x(g\theta - d_x v_x)) - k_3 v_x^{(2)} - k_2\dot{v}_x - k_1 v_x + k_1 v_{\text{lon}}\right] \tag{16}$$

$$= \left(a_{21} + \frac{J_{yy}}{g}(d_x^3 - k_3 d_x^2 + k_2 d_x - k_1)\right)v_x + \frac{J_{yy}}{g}\left(-d_x^2 g + k_3 d_x g - k_2 g\right)\theta + \left(b_{22} + J_{yy}(d_x - k_3)\right)q + \frac{J_{yy}}{g}k_1 v_{\text{lon}}. \tag{17}$$

This leads to

$$v_x^{(3)} = -k_3 v_x^{(2)} - k_2 v_x^{(1)} - k_1 v_x + k_1 v_{\text{lon}} \tag{18}$$

where k_1, k_2, and k_3 are chosen such that the following polynomial $s^3 + k_3 s^2 + k_2 s + k_1$ is Hurwitz, i.e., all roots of $Q(s) = s^3 + k_3 s^2 + k_2 s + k_1$ have negative real parts, so each solution of Eq. (18) asymptotically converges to the particular solution v_{lon} of the linear differential equation $Q(D)v_x = k_1 v_{\text{lon}}$ when v_{lon} is constant. We rewrite Eq. (16) more concisely as

$$u_2 = -K_{\text{lon}}X_{\text{lon}} + \frac{J_{yy}}{g}k_1 v_{\text{lon}} \tag{19}$$

with $X_{\text{lon}} = [v_x, \theta, q]^T$. The pre-stabilized X_{lon} subsystem from Eq. (12) with the choice from Eq. (19) is then rewritten as

$$\dot{X}_{\text{lon}} = A_{\text{lon}}X_{\text{lon}} + B_{\text{lon}}v_{\text{lon}} \tag{20}$$

Next, consider the case where v_{lon} is time-varying and satisfies $k_1 v_{\text{lon}}(t) = r_2(t)$ where in terms of Eq. (14),

$$r_2(t) = k_1 v_x^d + k_2 v_x^{(1),d} + k_3 v_x^{(2),d} + v_x^{(3),d} \tag{21}$$

$$= -k_1 k_p x + (-k_2 k_p + k_3 k_p d_x - k_p d_x^2)v_x + (-k_3 k_p g + k_p g d_x)\theta - k_p g q + k_1 k_p x_c + (k_1 + k_2 k_p)\dot{x}_c + (k_2 + k_p k_3)\ddot{x}_c + (k_p + k_3)x_c^{(3)} + x_c^{(4)}, \tag{22}$$

where the successive time derivatives $v_x^{(1),d}$, $v_x^{(2),d}$ and $v_x^{(3),d}$ of v_x^d were computed as follows using Eqs. (12) and (14):

$$v_x^{(1),d} = -k_p(\dot{x} - \dot{x}_c) + \ddot{x}_c = -k_p(v_x - \dot{x}_c) + \ddot{x}_c \tag{23}$$

$$v_x^{(2),d} = -k_p(\ddot{x} - \ddot{x}_c) + x_c^{(3)} = -k_p(g\theta - d_x v_x - \ddot{x}_c) + x_c^{(3)} \tag{24}$$

$$v_x^{(3),d} = -k_p(x^{(3)} - x_c^{(3)}) + x_c^{(4)} = -k_p(gq - d_x(g\theta - d_x v_x) - x_c^{(3)}) + x_c^{(4)} \tag{25}$$

Also, Eq. (18) with $k_1 v_{\text{lon}} = r_2(t)$ and Eq. (21) give $v_x^{(3)} = -k_3 v_x^{(2)} - k_2 v_x^{(1)} - k_1 v_x + k_1 v_x^d + k_2 v_x^{(1),d} + k_3 v_x^{(2),d} + v_x^{(3),d}$ and so also

$$v_x^{(3)} - v_x^{(3),d} = -k_3(v_x^{(2)} - v_x^{(2),d}) - k_2(v_x^{(1)} - v_x^{(1),d}) - k_1(v_x - v_x^d) \tag{26}$$

which, using Eqs. (2) and (14), can be rewritten as

$$\begin{aligned} x^{(4)} - (-k_p(x^{(3)} - x_c^{(3)}) + x_c^{(4)}) = & -k_3(x^{(3)} - (-k_p(\ddot{x} - \ddot{x}_c) + x_c^{(3)})) - k_2(x^{(2)} - (-k_p(\dot{x} - \dot{x}_c) + \ddot{x}_c)) \\ & -k_1(\dot{x} - \dot{x}_c + k_p(x - x_c)) \end{aligned} \tag{27}$$

which means that $x(t) - x_c(t)$ exponentially converges to 0 as $t \to +\infty$ when k_p, k_1, k_2, and k_3 are chosen such that all roots of the characteristic polynomial $s^4 + (k_3 + k_p)s^3 + (k_2 + k_3 k_p)s^2 + (k_1 + k_2 k_p)s + k_1 k_p$ for the $x - x_c$ dynamics have negative real parts.

Therefore, u_2 was designed such that when v_{lon} is constant, then v_x asymptotically tracks the constant v_{lon}, but when $k_1 v_{\text{lon}} = r_2(t)$, then x asymptotically tracks x_c.

2. Lateral tracking

One can derive the same type of velocity controller in the lateral plane by essentially replacing g by $-g$ in the calculations and use the lateral variables and Eqs. (11) and (13) instead of the longitudinal ones. Doing so, one gets:

$$\begin{aligned} u_1 = & \left(a_{12} + \frac{J_{xx}}{-g}(d_y^3 - k_3 d_y^2 + k_2 d_y - k_1)\right) v_y + \frac{J_{xx}}{-g}\left(-d_y^2(-g) + k_3 d_y(-g) - k_2(-g)\right)\phi \\ & + \left(b_{11} + J_{xx}(d_y - k_3)\right) p + \frac{J_{xx}}{-g} k_1 v_{\text{lat}} \end{aligned} \tag{28}$$

$$= -K_{\text{lat}} X_{\text{lat}} - \frac{J_{xx}}{g} k_1 v_{\text{lat}} \tag{29}$$

where $X_{\text{lat}} = [v_y, \phi, p]^T$. Again, y follows y_c when $k_1 v_{\text{lat}}(t) = r_1(t)$ where

$$\begin{aligned} r_1(t) = & -k_1 k_p y + (-k_2 k_p + k_3 k_p d_y - k_p d_y^2) v_y + (-k_3 k_p(-g) + k_p(-g) d_y)\phi - k_p(-g) p + k_1 k_p y_c \\ & + (k_1 + k_2 k_p)\dot{y}_c + (k_2 + k_p k_3)\ddot{y}_c + (k_p + k_3) y_c^{(3)} + y_c^{(4)} \end{aligned} \tag{30}$$

and where $v_y^d = -k_p(y - y_c) + \dot{y}_c$. The pre-stabilized lateral system is then finally denoted by:

$$\dot{X}_{\text{lat}} = A_{\text{lat}} X_{\text{lat}} + B_{\text{lat}} v_{\text{lat}} \tag{31}$$

C. Reformulation of the propellers thrust limitations as polynomial quadratic constraints

The collective thrust and torques are given by:

$$\begin{bmatrix} mc \\ \tau_1 \\ \tau_2 \\ \tau_3 \end{bmatrix} = M_{\text{eff}} \begin{bmatrix} T_1 \\ T_2 \\ T_3 \\ T_4 \end{bmatrix} \tag{32}$$

where T_i is the individual thrust of the rotor i, and where the control effectiveness matrix M_{eff} is invertible and is one of a quadrotor operating in the cross configuration:

$$M_{\text{eff}} = \begin{bmatrix} 1 & 1 & 1 & 1 \\ l & 0 & -l & 0 \\ 0 & -l & 0 & l \\ \rho & -\rho & \rho & -\rho \end{bmatrix} \tag{33}$$

where $l > 0$ is the length of each rotor from the center and $\rho = \frac{C_t}{C_m} > 0$ is the thrust to torque ratio of the rotor blades [2].

Each T_i is bounded within the range $[0, T_{max}]$, which by virtue of Eqs. (10)-(11), (19), and (29), means that the following constraints need to be satisfied:

$$M_{\text{eff}}^{-1}\begin{bmatrix} mc \\ \tau_1 \\ \tau_2 \\ \tau_3 \end{bmatrix} = M_{\text{eff}}^{-1}\begin{bmatrix} mg - md_x\theta v_x + md_y\phi v_y \\ -K_{\text{latt}}X_{\text{lat}} - \frac{J_{xx}}{g}k_1 v_{\text{lat}} + a_{11}v_x + b_{12}q + a_{13}(\theta v_x - \phi v_y) \\ -K_{\text{lon}}X_{\text{lon}} + \frac{J_{yy}}{g}k_1 v_{\text{lon}} + a_{22}v_y + b_{21}p + a_{23}(\theta v_x - \phi v_y) \\ a_{31}v_x + a_{32}v_y + a_{33}(\theta v_x - \phi v_y) \end{bmatrix} \in [0, T_{max}]^4 \tag{34}$$

Note that these constraints have both linear and quadratic terms in its variables X_{lon}, v_{lon}, X_{lat} and v_{lat}. This motivates our application of ideas from [27] for augmenting the state vector to convert nonlinear constraints into linear ones. We turn to this significant novel application next.

III. Reference governor design in the presence of polynomial constraints

A. Preliminaries

We next briefly summarize notation used in [27]. The Kronecker product of matrices A and B is denoted by $A \otimes B$. Given a vector $X \in \mathbb{R}^{n_x}$ for a positive integer p, its powers $X^{p\otimes} \in \mathbb{R}^{p n_x}$ are defined recursively using the Kronecker product of two column vectors. Since $X^{p\otimes}$ possesses repeated entries, we find it more convenient to use a vector X^p that removes the repeated components of $X^{p\otimes}$, i.e., X^p is a vector whose entries consist of all monomials $X_1^{i_1} \dots X_{n_x}^{i_x}$ for which the indices satisfy $i_1 + \dots + i_{n_x} = p$. The preceding relations were used to convert polynomial constraints into linear constraints in [27], which also entails augmenting the state space. We next illustrate how this can be done for the tracking problem we considered above, using a novel application of reference governors.

B. Problem position

Based on the previous section, we have these equations of motion when one applies the controllers (19) and (29):

$$\begin{cases} \dot{X}_{\text{lon}} &= A_{\text{lon}}X_{\text{lon}} + B_{\text{lon}}v_{\text{lon}} \\ \dot{X}_{\text{lat}} &= A_{\text{lat}}X_{\text{lat}} + B_{\text{lat}}v_{\text{lat}} \end{cases} \tag{35}$$

We can also add the reference dynamics when one designs the reference governor that is defined by

$$\dot{v}_{\text{lon}} = -\beta v_{\text{lon}} \quad \text{and} \quad \dot{v}_{\text{lat}} = -\beta v_{\text{lat}} \tag{36}$$

where $\beta > 0$ is a constant. The interpretation of the alternative add-on dynamics in Eq. (36) is as follows. The dynamics of v_{lon} and v_{lat} are as specified in the previous section when no constraint violations occur. Then, they switch to the dynamics in Eq. (36) when there is a constraint violation, and then they switch back to the dynamics from the previous section when the violations cease to occur. The drone will track the desired trajectory (x_c, y_c) when $k_1 v_{\text{lon}}(t) = r_2(t)$ and $k_1 v_{\text{lat}}(t) = r_1(t)$. Hence, the main idea of the reference governor method is to change the reference signal to the system from that of the nominal control whenever constraints are about to be violated according to Eq. (36) and remain inactive otherwise.

By Eq. (12) and Eq. (13), the position is computed from the velocities by using

$$\begin{cases} \dot{x} &= \begin{bmatrix} 1 & 0 & 0 \end{bmatrix} X_{\text{lon}} \\ \dot{y} &= \begin{bmatrix} 1 & 0 & 0 \end{bmatrix} X_{\text{lat}} \end{cases} \tag{37}$$

Here we follow the recently proposed method in [27] in order to consider polynomial constraints. The polynomial constraints (34) are quadratic, so the state is augmented with $[X_{\text{lon}}, v_{\text{lon}}, X_{\text{lat}}, v_{\text{lat}}]^2$. This gives a system of the form:

$$\dot{X}_v = \Phi X_v \tag{38}$$

where $X_v = [[X_{\text{lon}}, X_{\text{lat}}, v_{\text{lon}}, v_{\text{lat}}], [X_{\text{lon}}, X_{\text{lat}}, v_{\text{lon}}, v_{\text{lat}}]^2]$. Using this augmented state, the polynomial constraints (34) are now expressed as linear constraints.

C. Reference governor design

We use the reference governor design method that recently proposed in [27] after calculating the exact discretization of system Eq. (38) for a given sampling period. We recall here the main idea of the algorithm proposed in [27]. The reference governor design is based on the off-line calculation of two maximal output admissible sets (or MOAS).

- First, the MOAS O_{∞,Z_1} is computed for Eq. (35) subject to linear constraints. The linear constraints are simple min/max constraints on the pitch and roll angles, and collective thrust and torques. The calculation of this compact set makes it possible to determine bounds on each component of the augmented state X_v.
- Second, another MOAS, called $O_{\infty,Z}$, is computed for the pre-stabilized and augmented system in Eq. (38) subject to the original polynomial constraints in Eq. (34) (which are linear constraints of the augmented state) plus additional linear constraints which are defined by the bounds of the augmented state X_v.
- Finally, the reference governor solves a constrained nonlinear minimization problem at the initialization step (which can be done off-line for a grid of initial states) and then runs a bisection algorithm on-line at the subsequent time steps.

IV. Numerical results

We report numerical results when $d_x = 0.544$, $d_y = 0.236$, and the matrices A and B are all equal to zero. The sampling period is $10ms$ when one designs the reference governor for the discretization of the original continuous time model. Following Section III and the algorithm of [27], we choose $\beta = 0.98$ and first compute the MOAS O_{∞,Z_1} in the presence of the linear constraints. This set is finitely determined in $t^* = 84$ iterations and is defined by 252 non-redundant linear inequalities. Then, $O_{\infty,Z}$ is determined when we extend the state and add the nonlinear constraint. Here, $O_{\infty,Z}$ is determined in $t^* = 142$ iterations and is defined by 390 non-redundant linear inequalities.

In these simulations, the proposed reference governor is implemented and allows the thrust constraints $T_i \in [0, T_{\max}]$ to be satisfied for $i = 1, 2, 3, 4$, as well as the constraints $\theta \in [\theta_{\min}, \theta_{\max}]$ and $\phi \in [\phi_{\min}, \phi_{\max}]$ on the pitch and roll angles with $\phi_{\max} = \theta_{\max} = -\phi_{\min} = -\theta_{\min} = 25$deg. The maximum thrust of each propeller is $T_{\max} = 4.5N$. The gains of the nominal controllers are $k_p = 2$, $k_1 = 467$, $k_2 = 196$, and $k_3 = 24$. The reference trajectory is a circular one centered at $(0, 0)$ with $x_c(t) = R\cos(\omega t)$ and $y_c(t) = R\sin(\omega t)$ with $R = 1.8m$.

A. Starting close to the reference trajectory and following it at moderate speed

First, an angular speed of $\omega = 1$rad/s is chosen and the initial condition $[x(0), y(0)] = [x_c(0), y_c(0)] + [0.5, 0.5]$m near the desired reference trajectory is also chosen. The other state variables are initially at 0. Figure 2 indicates that the constrained variables are not in danger of being violated so that the reference governor is never activated and the reference trajectory is quickly followed as can be seen in Fig. 1. Figure 3 illustrates the tracking accuracy of the nominal controller. Here and in the sequel, we scale out the k_1 factor in the figures from the conditions on v_{lon} and v_{lat} when the reference governor is not active. Again, these results are only indicative of the performance of the nominal controller as the constraints are not in danger of being violated and thus, the reference governor remains inactive.

B. Starting far from the reference trajectory and following it at moderate speed

Secondly, we choose $\omega = 1$rad/s and an initial condition of $[x(0), y(0)] = [x_c(0), y_c(0)] + [2, 2]$m relatively far from the desired reference trajectory, as seen in Fig. 4. The other state variables are initially at 0. During the transient when the quadrotor UAV is far from the trajectory, the desire to move to the desired trajectory almost drives the vehicle to violate propeller thrust and pitch angle limits. It can be seen in Fig. 5 that during this time, the pitch angle and thrust approach their limits. The reference governor is activated during the transient to prevent the propeller thrusts and pitch angle from violating their limits and then the reference trajectory is correctly tracked. The deviation of the reference governor signal from that of the nominal governor is apparent during this time in Fig. 6.

C. Starting close to the reference trajectory and following it at high speed

Third, we choose $\omega = 2$rad/s, which is quite large, and an initial condition $[x(0), y(0)] = [x_c(0), y_c(0)] + [0.5, 0.5]$m close to the desired trajectory. The other state variables are initially at 0. Figure 8 indicates the reference governor is frequently activated to prevent the propeller thrusts, pitch and roll angles from violating their limits and the reference trajectory is no longer tracked accurately. Comparison of the reference signals in Fig. 9 indicates that the changing reference signal of the nominal controller consistently drives the constraints to be violated. The reference governor is successful in ensuring that these constraints are satisfied at the cost of the accuracy of the trajectory following.

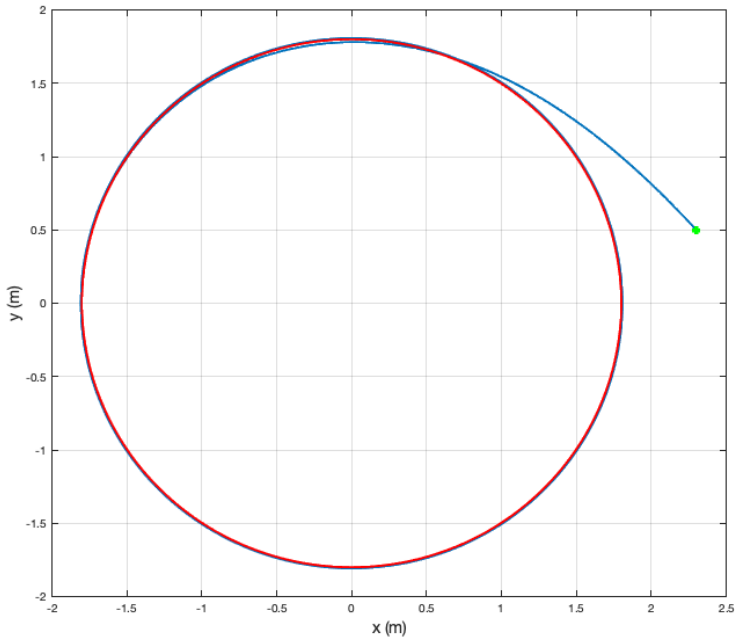

Fig. 1 Trajectory tracking starting from $[x(0), y(0)] = [2.3, 0.5]m$

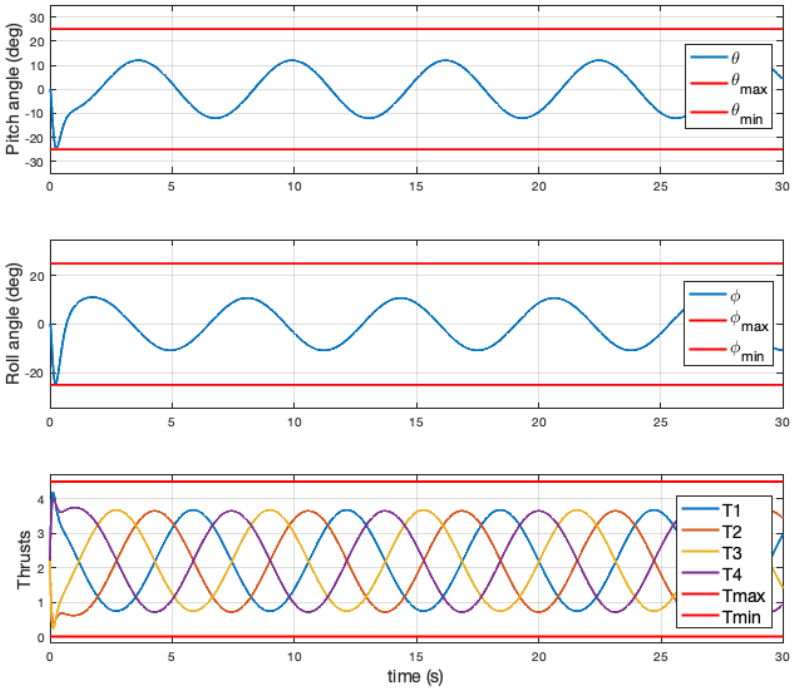

Fig. 2 Constrained variables starting from $[x(0), y(0)] = [2.3, 0.5]m$

Interestingly, it can be seen in Fig. 7 that the drone finally seems to follow smaller and almost circular trajectories at the high speed $\omega = 2\text{rad/s}$.

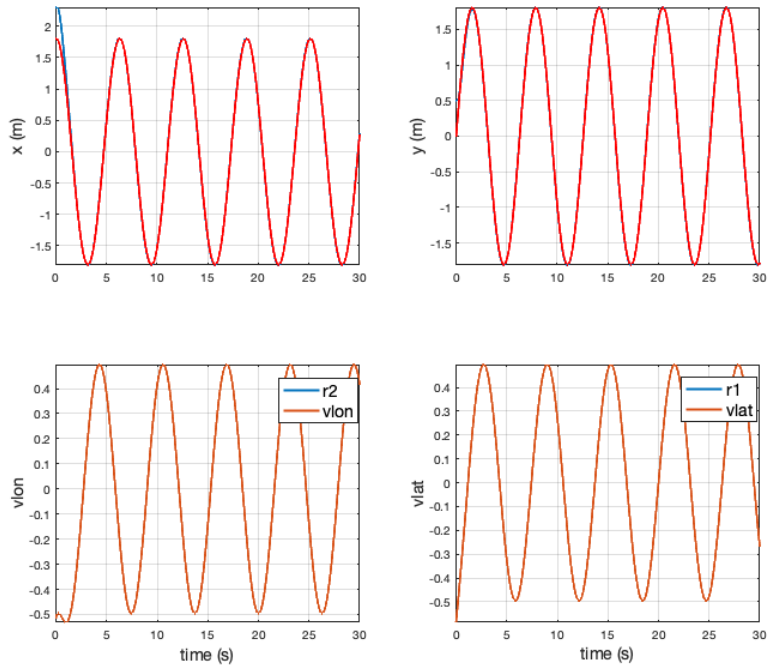

Fig. 3 (x, y) **tracking and time evolution of the references** v_{lon} **and** v_{lat} **starting from** $[x(0), y(0)] = [2.3, 0.5]$**m, with** r_1 **and** r_2 **scaled by** $1/k_1$

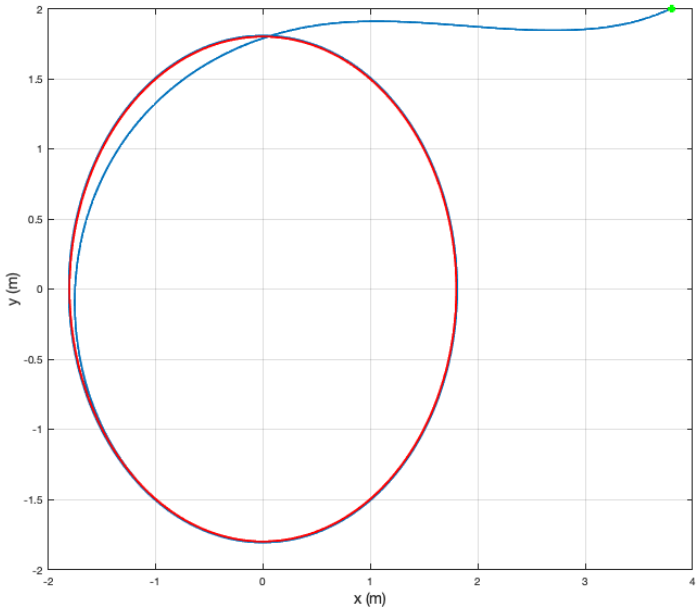

Fig. 4 **Trajectory tracking starting from** $[x(0), y(0)] = [3.8, 2]m$

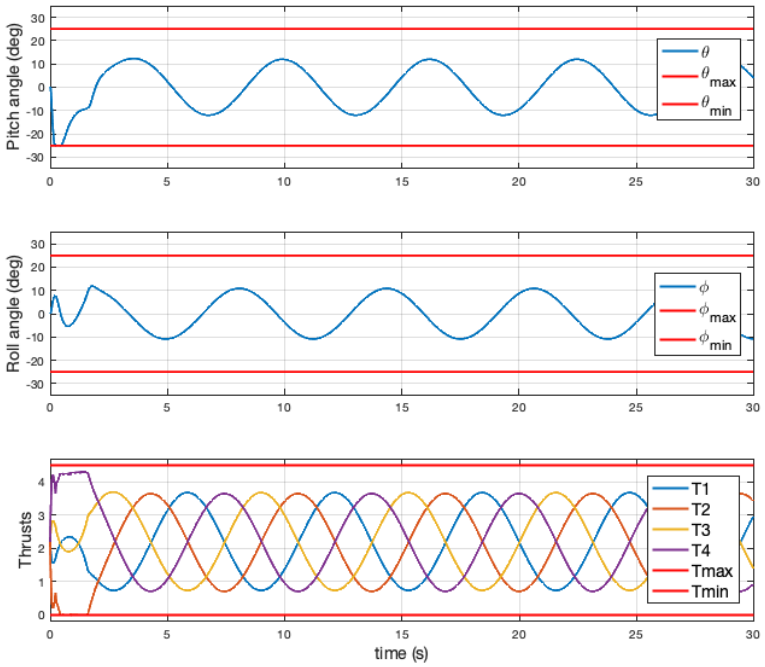

Fig. 5 Constrained variables starting from $[x(0), y(0)] = [3.8, 2]m$

V. Conclusions

We demonstrated the value of state augmentation and reference governor approaches from [27]. For the first time, we used these methods for flight envelope protection while following high-speed trajectories. The method proposed is based on the computation a safe forward invariant set in which the state (and reference) of the quadrotor must remain while tracking a circular trajectory. The safe forward invariant set is also referred to as the maximum output admissible set (or MOAS) in the reference governor literature. In the future, we plan to extend our results to cases where we must follow more complex trajectories and/or have modeling uncertainties and/or have wind disturbances. Also, we plan to work on the real-time implementation of the proposed control algorithms on a physical drone.

Acknowledgments

This research is supported by the Office of Naval Research (ONR) under award N00014-22-1-2135. Rick Schieni is also supported by the Middlesex College, NJ, USA.

References

[1] Faessler, M., Franchi, A., and Scaramuzza, D., "Differential flatness of quadrotor dynamics subject to rotor drag for accurate tracking of high-speed trajectories," *IEEE Robotics and Automation Letters*, Vol. 3, No. 2, 2018, pp. 620–626. https://doi.org/10.1109/LRA.2017.2776353.

[2] Svacha, J., Mohta, K., and Kumar, V., "Improving quadrotor trajectory tracking by compensating for aerodynamic effects," *Proceedings of the International Conference on Unmanned Aircraft Systems*, 2017, pp. 860–866. https://doi.org/10.1109/ICUAS.2017.7991501.

[3] Johnson, W., *Helicopter Theory*, Princeton University Press, Princeton, N.J, 1980.

[4] Leishman, J. G., *Principles of Helicopter Aerodynamics*, Cambridge Aerospace Series 12, Cambridge University Press, Cambridge, UK, 2000.

[5] Kroo, I., Prinz, F., Shantz, M., Kunz, P., Fay, G., Cheng, S., Fabian, T., and Partridge, C., "The Mesicopter: A miniature

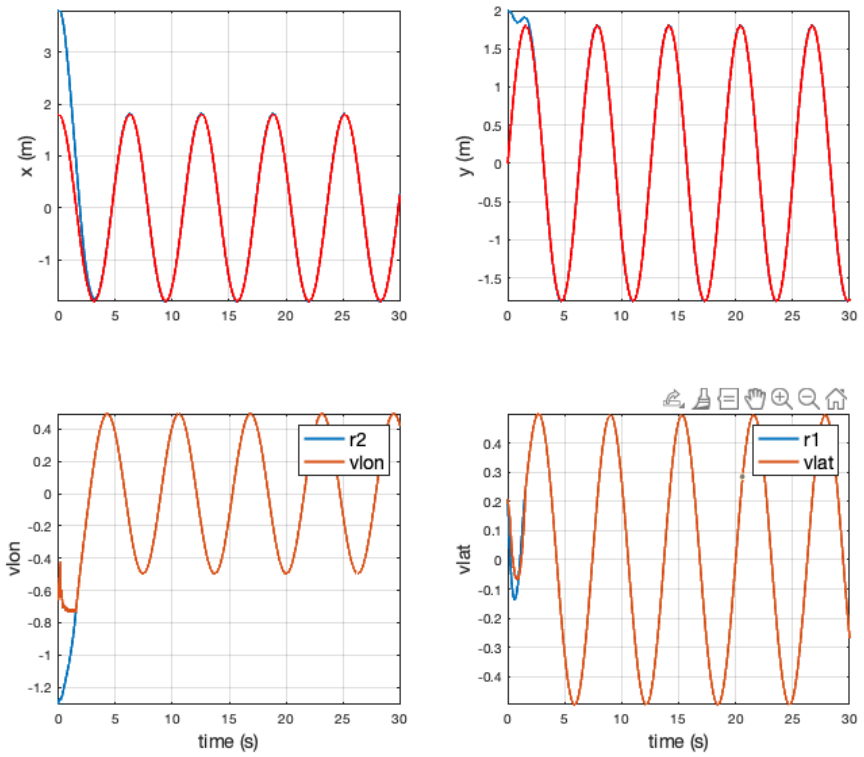

Fig. 6 (x, y) **tracking and time evolution of the references** v_{lon} **and** v_{lat} **starting from** $[x(0), y(0)] = [3.8, 2]m$**, with** r_1 **and** r_2 **scaled by** $1/k_1$

rotorcraft concept phase II: interim report," *Stanford University*, 2000. URL http://www.niac.usra.edu/files/studies/final_report/377Kroo.pdf.

[6] Mokhtari, A., and Benallegue, A., "Dynamic feedback controller of Euler angles and wind parameters estimation for a quadrotor unmanned aerial vehicle," *Proceedings of the IEEE International Conference on Robotics and Automation*, Vol. 3, 2004, pp. 2359–2366. https://doi.org/10.1109/ROBOT.2004.1307414.

[7] Kai, J.-M., Allibert, G., Hua, M.-D., and Hamel, T., "Nonlinear feedback control of quadrotors exploiting first-order drag effects," *IFAC-PapersOnLine*, Vol. 50, No. 1, 2017, pp. 8189–8195. https://doi.org/10.1016/j.ifacol.2017.08.1267.

[8] Pounds, P., Mahony, R., and Corke, P., "Modelling and control of a large quadrotor robot," *Control Engineering Practice*, Vol. 18, No. 7, 2010, pp. 691–699. https://doi.org/10.1016/j.conengprac.2010.02.008.

[9] Martin, P., and Salaün, E., "The true role of accelerometer feedback in quadrotor control," *Proceedings of the IEEE International Conference on Robotics and Automation*, 2010, pp. 1623–1629. https://doi.org/10.1109/ROBOT.2010.5509980.

[10] du Plessis, J., and Pounds, P., "Rotor flapping for a triangular quadrotor," *Proceedings of the Australiasian Conference on Robotics and Automation*, 2014, pp. 1–7.

[11] Pounds, P., Mahony, R., and Corke, P., "Modelling and control of a quad-rotor robot," *Proceedings of the 2006 Australasian Conference on Robotics and Automation*, 2006, pp. 1–10.

[12] Hoffmann, G., Huang, H., Waslander, S., and Tomlin, C., "Quadrotor helicopter flight dynamics and control: theory and experiment," *Proceedings of the AIAA Guidance, Navigation and Control Conference and Exhibit*, 2007, pp. 1–20. https://doi.org/10.2514/6.2007-6461.

[13] Huang, H., Hoffmann, G. M., Waslander, S. L., and Tomlin, C. J., "Aerodynamics and control of autonomous quadrotor helicopters in aggressive maneuvering," *Proceedings of the IEEE International Conference on Robotics and Automation*, 2009, pp. 3277–3282. https://doi.org/10.1109/ROBOT.2009.5152561.

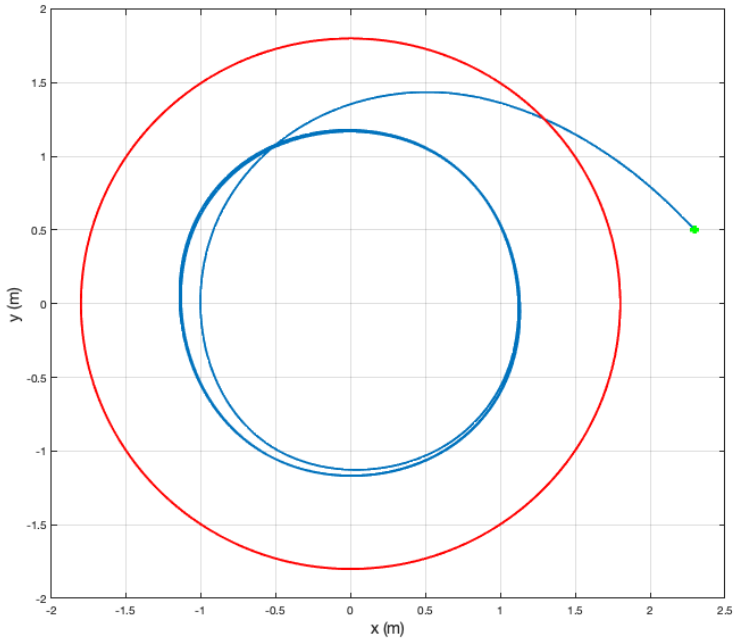

Fig. 7 Trajectory tracking starting from $[x(0), y(0)] = [2.3, 0.5]m$

[14] Bristeau, P.-J., Martin, P., Salaün, E., and Petit, N., "The role of propeller aerodynamics in the model of a quadrotor UAV," *Proceedings of the European Control Conference*, 2009, pp. 683–688. https://doi.org/10.23919/ECC.2009.7074482.

[15] Omari, S., Hua, M.-D., Ducard, G., and Hamel, T., "Nonlinear control of VTOL UAVs incorporating flapping dynamics," *Proceedings of the IEEE/RSJ International Conference on Intelligent Robots and Systems*, 2013, pp. 2419–2425. https://doi.org/10.1109/IROS.2013.6696696.

[16] Belcastro, C. M., Newman, R. L., Evans, J., Klyde, D. H., Barr, L. C., and Ancel, E., "Hazards identification and analysis for unmanned aircraft system operations," *Proceedings of the 17th AIAA Aviation Technology, Integration, and Operations Conference*, 2017. https://doi.org/10.2514/6.2017-3269.

[17] Briere, D., and Traverse, P., "AIRBUS A320/A330/A340 electrical flight controls - A family of fault-tolerant systems," *Proceedings of the 23rd International Symposium on Fault-Tolerant Computing*, 1993, pp. 616–623. https://doi.org/10.1109/FTCS.1993.627364.

[18] Wilborn, J., and Foster, J., "Defining commercial transport loss-of-control: A quantitative approach," *Proceedings of the AIAA Atmospheric Flight Mechanics Conference and Exhibit*, 2004. https://doi.org/10.2514/6.2004-4811.

[19] Chongvisal, J., Tekles, N., Xargay, E., Talleur, D., Kirlik, A., and Hovakimyan, N., "Loss-of-control prediction and prevention for NASA's transport class model," *Proceedings of the AIAA Guidance, Navigation, and Control Conference*, 2014, pp. 1–31. https://doi.org/10.2514/6.2014-0784.

[20] Pfifer, H., Venkataraman, R., and Seiler, P., "Quantifying loss-of-control envelopes via robust tracking analysis," *Journal of Guidance, Control, and Dynamics*, Vol. 40, No. 4, 2017, pp. 1042–1050. https://doi.org/10.2514/1.G001748.

[21] Sun, S., and de Visser, C. C., "Quadrotor safe flight envelope prediction in the high-speed regime: A Monte-Carlo approach," *Proceedings of the AIAA Scitech Forum*, 2019. https://doi.org/10.2514/6.2019-0948, Paper AIAA 2019-0948.

[22] Garone, E., Cairano, S. D., and Kolmanovsky, I., "Reference and command governors for systems with constraints: A survey on theory and applications," *Automatica*, Vol. 75, 2017, pp. 306–328. https://doi.org/10.1016/j.automatica.2016.08.013.

[23] Kolmanovsky, I., Garone, E., and Di Cairano, S., "Reference and command governors: A tutorial on their theory and automotive applications," *Proceedings of the American Control Conference*, 2014, pp. 226–241. https://doi.org/10.1109/ACC.2014.6859176.

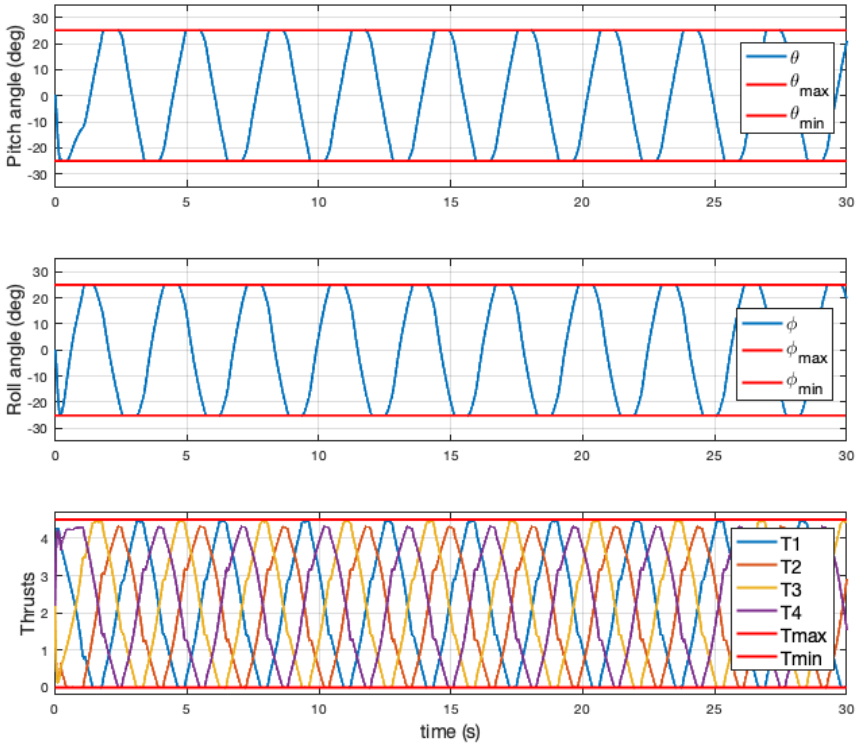

Fig. 8 Constrained variables starting from $[x(0), y(0)] = [2.3, 0.5]m$

[24] Bencatel, R., Tian, R., Girard, A. R., and Kolmanovsky, I., "Reference governor strategies for vehicle rollover avoidance," *IEEE Transactions on Control Systems Technology*, Vol. 26, No. 6, 2018, pp. 1954–1969. https://doi.org/10.1109/TCST.2017.2753168.

[25] Liu, K., Li, N., Kolmanovsky, I., Rizzo, D., and Girard, A., "Safe learning reference governor: theory and application to fuel truck rollover avoidance," *Journal of Autonomous Vehicles and Systems*, Vol. 1, No. 4, Paper 041003, 2022. https://doi.org/10.1115/1.4053244.

[26] Higgins, M. R., and Burlion, L., "Implementation of a learning-based explicit reference governor for constrained control of a UAV," *Proceedings of the AIAA SCITECH Forum*, 2022, Paper AIAA 2022-2042. https://doi.org/10.2514/6.2022-2042.

[27] Burlion, L., Schieni, R., and Kolmanovsky, I. V., "A reference governor for linear systems with polynomial constraints," *Automatica*, Vol. 143, No. 110313, 2022. https://doi.org/10.1016/j.automatica.2022.110313.

[28] Schieni, R., and Burlion, L., "A reference governor for control of bistable structures with polynomial constraints," *Proceedings of the IEEE Conference on Control Technology and Applications*, 2022, to appear.

[29] Prouty, R., *Helicopter Performance, Stability, and Control*, Krieger, Malabar, FL, 2005. URL https://books.google.com/books?id=WvyHQAAACAAJ.

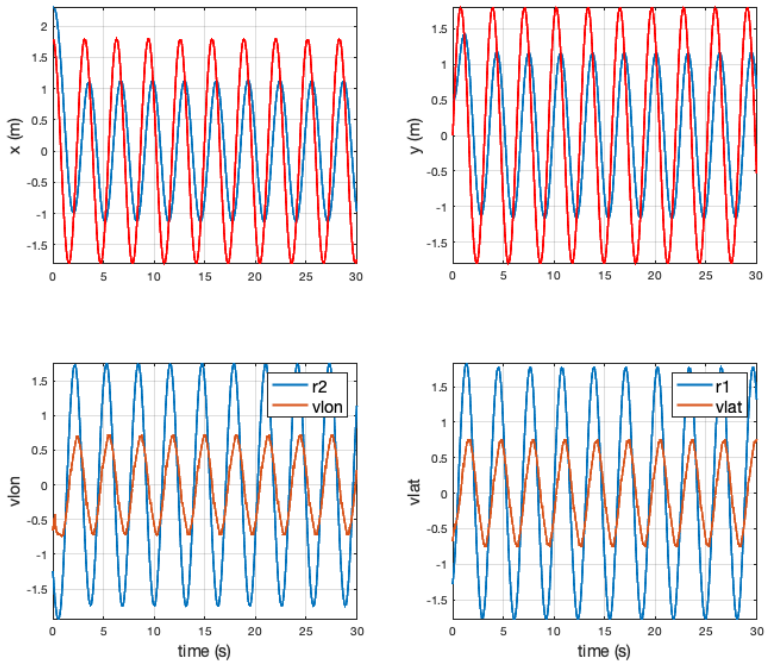

Fig. 9 (x, y) **tracking and time evolution of references** v_{lon} **and** v_{lat} **starting from** $[x(0), y(0)] = [2.3, 0.5]m$**, with** r_1 **and** r_2 **scaled by** $1/k_1$